Available online at www.sciencedirect.com
SCIENCE DIRECT®
International Journal of Heat and Fluid Flow 24 (2003) 470–479
International Journal of HEAT AND FLUID FLOW
www.elsevier.com/locate/ijhff

LES, coarse LES, and transient RANS comparisons on the flow across a tube bundle

S. Benhamadouche [a,b], D. Laurence [a,b,*]

[a] Electricité de France R&D, MFTT, 6 Quai Watier, 78400 Chatou, France
[b] Department of Mechanical, Aerospace & Manufacturing Engineering, MAME Thermofluids Division, UMIST, P.O. Box 88, Manchester M60 1QD, UK

Received 15 December 2002; accepted 15 March 2003

Abstract

The cross-flow in a staggered tube bundle is computed with an LES and a transient Reynolds stress transport model (RSTM) in 2D and 3D, with two levels of grid refinement. The numerical method is based on a finite volume approach on unstructured grids using a collocated arrangement for all the unknowns. It is shown that the LES results on the fine mesh are comparable to a DNS and experiments and reasonable agreement is still achieved with a coarse mesh. The RSTM also produced satisfactory results in 3D but showed no advantage over the LES when the grid was coarsened. The 2D RSTM, which produced strong vortex shedding, was found to be physically unreasonable.

Keywords: LES; RSTM; TRANS; Tube bundle; Finite volume method

1. Introduction

Heat exchangers are vital components of power generation systems, which present many issues that are not understood in detail and others that need to be optimized. These include heat transfer enhancement vs. head loss, hot spots, vibrations, fluid structure coupling, two phase flows and dust deposition, etc.

A major parametric CFD study of tube bundles would seem timely and worthwhile in view of the billion $/year potential savings worldwide, for coal power plants alone (Bouris et al., 2001). However, Reynolds averaged Navier–Stokes (RANS) simulations have so far failed to produce reliable predictions of flows across tube bundles.

This provocative statement is based on numerous reported RANS simulations: the ERCOFTAC workshops on refined flow modeling of 1993 and 1994 (Rollet-Miet et al., 1999; Sebag et al., 1991; Meyer, 1994; Bouris and Bergeles, 1999). The general conclusion is that even advanced RANS models such as non-linear, realizable and RNG types of k–epsilon models severely underestimate the high turbulent kinetic energy levels observed in densely packed tube bundles. The same can be said of Reynolds stress transport models (RSTM), though the underestimation is somewhat less severe (especially when non-standard coefficients are used, Sebag, 1991). Paradoxically the standard k–epsilon model returns reasonable predictions of mean velocities and global level of turbulent kinetic energy, but this is purely by chance thanks to the erroneous overproduction of kinetic energy on the impinging side of the tubes. This artificially raises the overall turbulence intensity but the locations of the maximum and minimum are erroneous.

These discrepancies have led Hassan and Ibrahim (1997), Bouris et al. (2001), Bouris and Bergeles (1999), to resort to "two dimensional LES" with some success including the prediction of turbulence levels. However debatable this approach may be, it yielded better results for the mean velocities and turbulent kinetic energy than RANS models, thus allowing some analysis of stress loading, heat transfer and deposition rates which are highly dependent on the turbulence intensity.

This paper is a follow-up of the work at EDF by Rollet-Miet et al. (1999) who applied an industrial finite

* Corresponding author. Tel.: +44-161-200-3704; fax: +44-161-200-3723.
E-mail address: dominique.laurence@umist.ac.uk (D. Laurence).

0142-727X/03/$ - see front matter © 2003 Elsevier Science Inc. All rights reserved.
doi:10.1016/S0142-727X(03)00060-2

element code, N3S, to 3D LES of the flow in a staggered tube bundle, obtained surprisingly good results and observed that the subgrid scale model (whether Smagorinsky or dynamic) had very little effect. The present simulations are based on a new unstructured finite volume code, *Code_Saturne* ®. When the LES modules were implemented in this new code, the preliminary test cases of Rollet-Miet et al. (1999) were successfully simulated but are not reported herein. The paper reports the effect of mesh refinement on two LES simulations, comparisons with 2D and 3D transient RSTM simulations, and an independent DNS.

2. Numerical method

The flow is assumed incompressible and Newtonian and the density is constant. Let $\underline{\bar{u}}$ be the filtered velocity when using LES and the mean value of the velocity for RSTM.

The filtered (resp. Reynolds averaged) Navier–Stokes equations can be written for LES (resp. RSTM):

$$\begin{cases} \dfrac{\partial \bar{u}_i}{\partial t} + \dfrac{\partial \bar{u}_i \bar{u}_j}{\partial x_j} = -\dfrac{1}{\rho}\dfrac{\partial \bar{p}}{\partial x_i} + \nu \dfrac{\partial^2 \bar{u}_i}{\partial x_j \partial x_j} - \dfrac{\partial \tau_{ij}}{\partial x_j}, \\ \quad i \in \{1,2,3\} \\ \dfrac{\partial \bar{u}_j}{\partial x_j} = 0 \end{cases} \tag{1}$$

2.1. LES

As Rollet-Miet et al. (1999) have shown that the subgrid model is not crucial in the tube bundle case, only the classical Smagorinsky model is used:

$$\begin{cases} \tau_{ij} = \overline{u_i u_j} - \bar{u}_i \bar{u}_j \\ \tau_{ij} - \frac{1}{3}\tau_{kk}\delta_{ij} = -2\nu_t \bar{S}_{ij} = -2(C_S \bar{\Delta})^2 \|S\| \bar{S}_{ij} \end{cases} \tag{2}$$

$\bar{S}_{ij}$ is the filtered strain rate tensor ($\|S\| = \sqrt{2\bar{S}_{ij}\bar{S}_{ij}}$), ν_t the subgrid turbulent viscosity and $\bar{\Delta}$ the length scale of the filter. As the cells used in the present work are hexahedral, one can take $\bar{\Delta} = 2\Omega^{1/3}$, where Ω is the volume of a cell. The Smagorinsky constant, C_S, is set to 0.065.

2.2. RSTM

When using RSTM model, in Navier–Stokes equations, $\underline{\underline{\tau}}$ in (1) replaced by $\underline{\underline{R}}$, the Reynolds stress tensor. The Reynolds stresses are governed by the following equations:

$$\frac{\partial R_{ij}}{\partial t} + \frac{\partial R_{ij}\bar{u}_k}{\partial x_k} = P_{ij} + \Phi_{ij} + d_{ij} - \varepsilon_{ij} \tag{3}$$

Following Launder et al. (1975), the pressure–strain correlation associated with the deviatoric part of $\underline{\underline{\varepsilon}}$ is decomposed into three terms:

$$\Phi_{ij} - \left(\varepsilon_{ij} - \tfrac{2}{3}\varepsilon\delta_{ij}\right) = \varphi_{ij,1} + \varphi_{ij,2} + \varphi_{ij,w}$$

$\varphi_{ij,w}$ is a wall echo term (see Gibson and Launder, 1978) and is neglected in the present work.

$$\begin{cases} \varphi_{ij,1} = -C_1 \frac{\varepsilon}{k}\left(R_{ij} - \frac{2}{3}k\delta_{ij}\right): \\ \quad \text{slow term (return to isotropy)} \\ \varphi_{ij,2} = -C_2\left(P_{ij} - \frac{2}{3}P\delta_{ij}\right): \\ \quad \text{rapid term (isotropization of the production)} \end{cases}$$

Following Daly and Harlow (1970), the diffusive transport of the Reynolds stresses and the dissipation rate are described with a tensorial model:

$$d_{ij} = C'_S \frac{\partial}{\partial x_k}\left(\frac{k}{\varepsilon} R_{km} \frac{\partial R_{ij}}{\partial x_m}\right) + \frac{\partial}{\partial x_k}\left(\nu \frac{\partial R_{ij}}{\partial x_k}\right)$$

The equation for the dissipation rate ε is

$$\frac{\partial \varepsilon}{\partial t} + \frac{\partial \varepsilon \bar{u}_j}{\partial x_j} = C_\varepsilon \frac{\partial}{\partial x_k}\left(\frac{k}{\varepsilon} R_{km} \frac{\partial \varepsilon}{\partial x_m}\right) + C_{\varepsilon 1}\frac{\varepsilon}{k}P - C_{\varepsilon 2}\frac{\varepsilon^2}{k} + \nu \frac{\partial^2 \varepsilon}{\partial x_j \partial x_j}$$

The standard values of constants are used:

$$C_1 = 1.8, \quad C_2 = 0.6, \quad C'_S = 0.22,$$
$$C_\varepsilon = 0.18, \quad C_{\varepsilon 1} = 1.44, \quad C_{\varepsilon 2} = 1.92.$$

2.3. Numerical method

A finite volume code for complex geometries, *Code_Saturne* ® (Archambeau et al., 2003), is used to solve the previous equations on unstructured grids. In the collocated finite volume approach used here, all variables are located at the centers of gravity of the cells (which can be of any shape). The momentum equations are solved by considering an explicit mass flux (the three components of the velocity are thus uncoupled). Velocity and pressure coupling is insured by a prediction/correction method with a SIMPLEC algorithm (Ferziger and Perić, 1999). The Poisson equation is solved with a conjugate gradient method. The collocated discretisation requires a Rhie and Chow (1982) interpolation in the correction step to avoid oscillatory solutions. This interpolation has been used in the present work although it does not seem essential for unstructured meshes.

For the LES calculations a second order centered scheme (in space and time) is used. It is Crank–Nicolson (CN) in time with linearized convection, and the second order Adams–Bashforth (AB) method is used for the part of the diffusion involving the transposed gradient operator, that couples the velocity components.

That is,

$$\text{in} \quad \frac{\partial \bar{u}_i \bar{u}_j}{\partial x_j} \quad \text{and in} \quad \frac{\partial}{\partial x_j}\left[\nu_t\left(\frac{\partial \bar{u}_i}{\partial x_j} + \frac{\partial \bar{u}_j}{\partial x_i}\right)\right]$$

AB is applied to $\bar{u}_j$ and CN to $\bar{u}_i$.

For the transient RANS calculations, the Euler implicit (first order) upwind scheme is used for the turbulent variables, but the second order centered convection scheme is used for the velocity components. This is a major difference with the other RANS calculations mentioned in Section 1.

The present test case requires only periodic and wall boundary conditions. The LES uses a Werner and Wengle (1991) (power law) wall function and the RSTM uses standard wall functions.

3. Flow in the tube bundle

Fig. 1 shows the computational domain, a subset of the tube bundle experiment of Simonin and Barcouda (1988). The tube diameter is $D = 22{,}7$ mm and length is $L = 45$ mm. The measurements provide data for the mean velocities and Reynolds stresses at several locations, and three profiles, as indicated in Fig. 2, are chosen for comparisons. Moulinec et al. (2001) performed a DNS on this test case and their results are included for comparisons.

Two meshes (Figs. 3 and 4) have been used, a coarse one with 2016 cells on each of nine planes in the third direction and a fine one with 8872 cells in 2D, times 20 planes in the third direction. The "coarse" mesh in the present LES computation has a total of 18 000 cells, about 10 times less than the "fine" mesh which has 170 000 cells. This latter "fine" mesh is similar, if not more accurate, to the 280 000 cells mesh used in the LES by Rollet-Miet et al. (1999), because one Finite Volume hexa cell corresponds to 5 or 6 Finite Element Tetra cells. Moulinec et al. (2001) used 5 Million cells in their DNS.

In the "2D" calculations the same meshes but restricted to one (x, y) plane are used (Figs. 3 and 4). For all cases, the maximum CFL number is below unity and its time average is between 0.3 and 0.5. The mean values

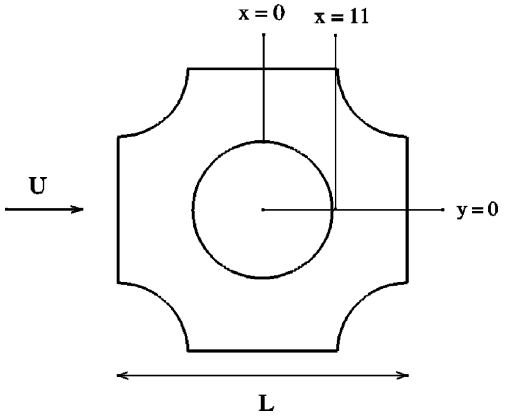

Fig. 2. Profiles location.

are averaged over time, and in the third direction in the 3D cases.

In the experiment, the Reynolds number based on the bulk velocity and tube diameter ($Re = UD/\nu$) was 18 000. The Reynolds number considered in the present work is 9000. Rollet-Miet et al. (1999) and Moulinec et al. (2001) used Re values of 7000 and 6000 respectively. Despite this, the results will be shown to be comparable. In the core of the flow, the ratio of eddy viscosity to molecular viscosity is on average 15 for the coarse mesh and 7 for the fine mesh. Hence the only area where the actual Re number may play a significant role is in the near wall cells. For the coarse LES, 99% of these cells exhibit a $y+$ value below 11. For the fine LES 100% of the cells are below $y+ = 7$. As the flow along the tubes is dominated by impingement and separation it was felt preferable to distort the Re number to avoid relying on equilibrium boundary layer assumptions entailed by use of wall functions above the viscous layer.

The level of turbulence intensity is very high (35%) and is produced mainly in the free shear layers, which

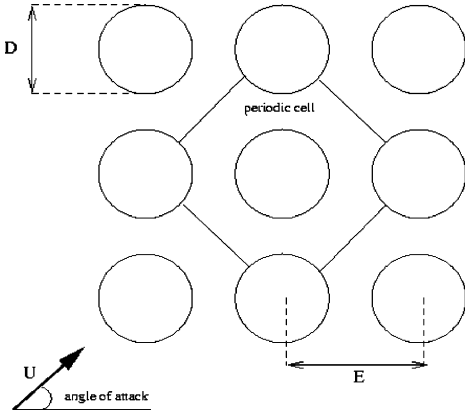

Fig. 1. Square tube bundle.

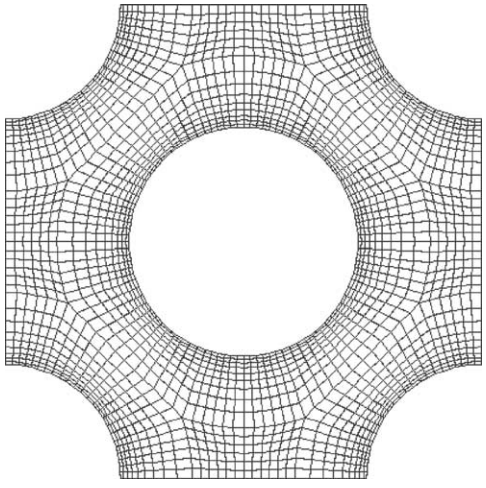

Fig. 3. The coarse mesh (2D visualizations).

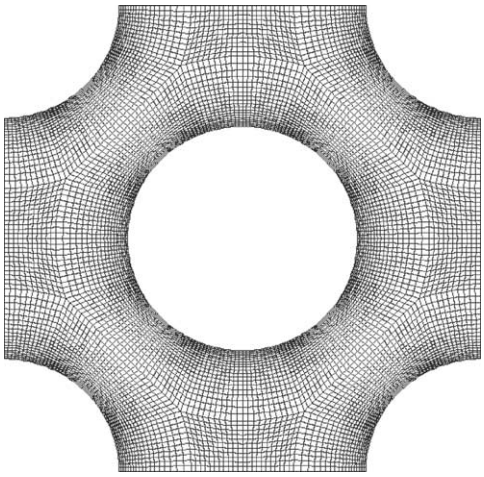

Fig. 4. The fine mesh (2D visualization).

further limits the effects of *Re* number and near-wall modeling. In addition, Moulinec et al. (in press) have shown that the length of the recirculation zone has an asymptotic behavior for high Reynolds numbers (the value is constant after Reynolds 500).

3.1. 3D calculations

Figs. 5–7 show LES and RSTM results obtained with the fine grid. The results of LES are comparable to those of the DNS, as Moulinec et al. (2001) reported. The RSTM in 3D yields an unsteady solution as a consequence of the progression of numerical methods toward lower numerical diffusion. The previous RANS calculations mentioned in the introduction mainly used steady-state algorithms, but others that used unsteady methods converged to a steady-state even with advanced RSTM models. The present 2D and 3D RSTM simulations remained transient, possibly due to the accurate non-diffusive periodicity conditions developed for the LES (the periodic conditions are fully implicit, the boundary faces are treated like the internal ones). The results are thus processed as a T-RANS (Transient RANS) in the sense of Kenjeres and Hanjalic (1999). The contribution of the coherent or resolved part of the velocity fluctuations is added to the Reynolds stresses in Figs. 5–7 ($\overline{u_iu_j}|_{\text{tot}} = \overline{R}_{ij}|_{\text{model}} + \overline{u_iu_j}|_{\text{resolved}}$).

The results are quite satisfactory whereas previous steady-state RANS simulations yielded poor results as reported by Rollet-Miet et al. (1999) and Sebag et al. (1991). The DNS and LES results produced by three different codes agree fairly well with each other (Rollet-Miet et al. with finite elements, Moulinec et al. with finite differences, and the present finite volume LES), but seem to overestimate slightly the mean velocity on the side of the tube ($x = 0$ and 11). There is also an overestimation of the streamwise fluctuations, $\overline{u'^2}$, in all simulations including the RSTM. The latter does not predict well the variation of $\overline{u'^2}$ also along $x = 11$ which crosses the flow from the rear of one cylinder to the front and the stagnation point of the next. At the same location, both LES and RSTM underestimate the wall parallel component of the fluctuations, $\overline{v'^2}$. The dip in $\overline{u'^2}$ and peak in $\overline{v'^2}$ is interpreted as a near wall redistribution

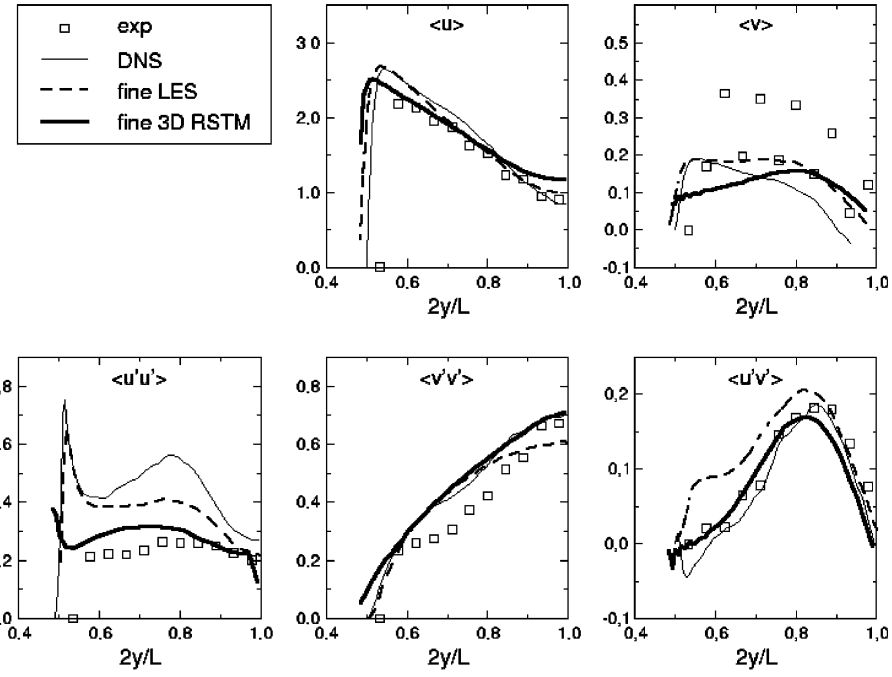

Fig. 5. LES and RSTM (3D) profiles ($x = 0$).

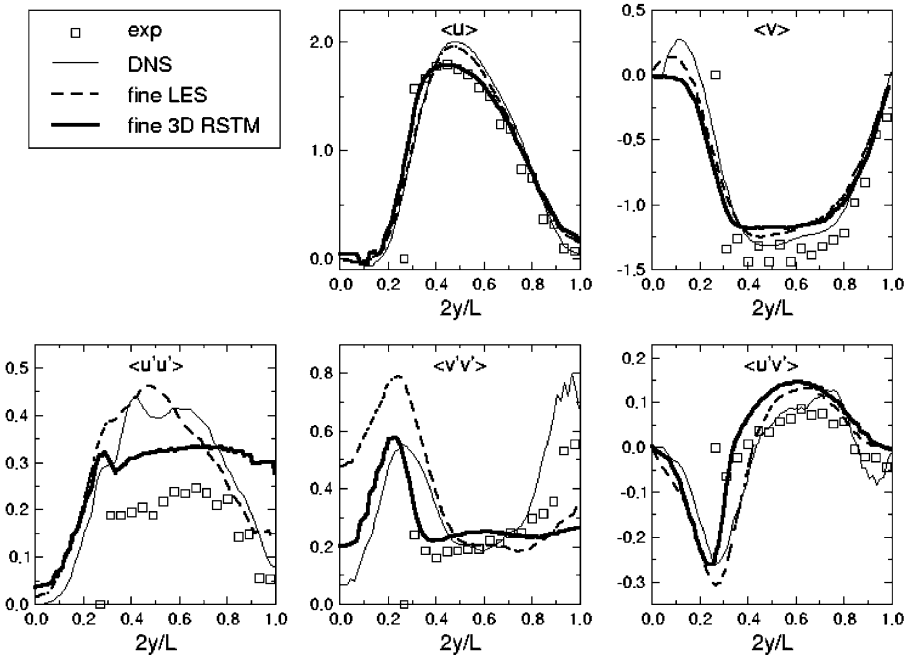

Fig. 6. LES and RSTM (3D) profiles ($x = 11$).

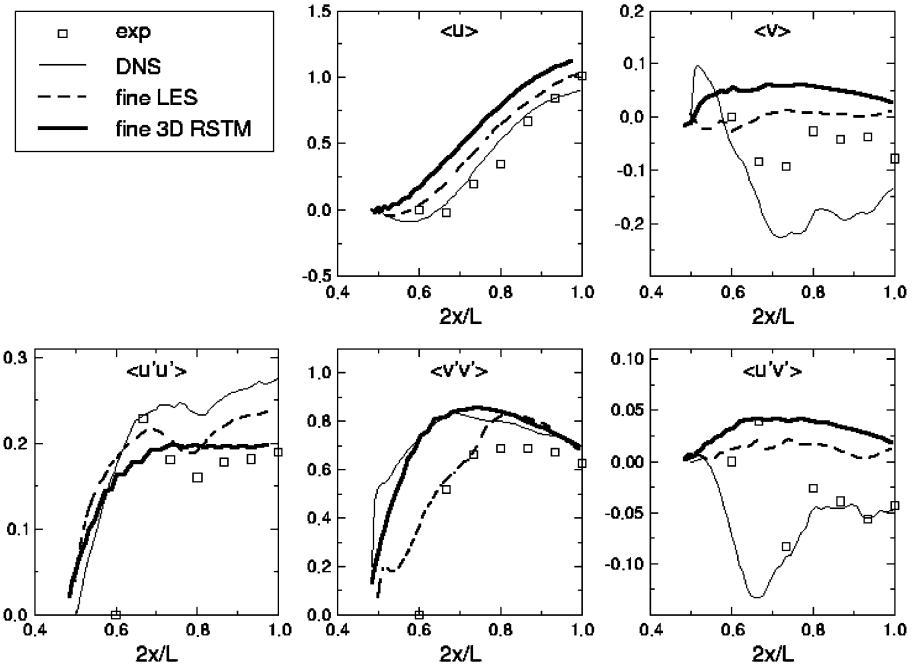

Fig. 7. LES and RSTM (3D) profiles ($y = 0$).

effect that is only well reproduced on a very fine mesh used by the DNS. In Rollet-Miet et al. this is the only location where the dynamic and Smagorinsky models differed. The latter yielded a negative average eddy viscosity, which is perhaps an indication of the need for local mesh refinement.

The short mean recirculation zone can be seen in the profile at $y = 0$. No mean recirculation is found with the RSTM model and the LES underestimate the length of this zone. For symmetry reasons, V and $\overline{u'v'}$ should be zero at $y = 0$. Experiments show that the flow occasionally and randomly switches mean directions and can take a 45° orientation. This strange phenomenon appears on several different rigs and even more frequently in the tubes-in-line configuration. It is possible that the present staggered configuration occasionally bifurcates

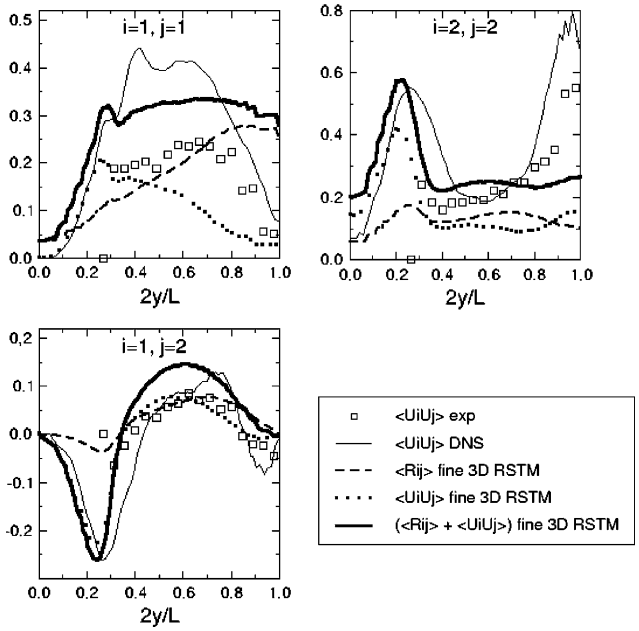

Fig. 8. RSTM (3D fine) calculation ($x = 11$)—comparison of the Reynolds stresses vs. the coherent part of the stresses.

to in-line flow configuration. With the periodic conditions imposed in the simulation, nothing prevents a non-zero net flow-rate in the lateral direction (other than minimization of head losses). Averaging over longer periods of time reduces this bias however (DNS statistics were gathered over a shorter period than the present LES).

The Reynolds stresses are decomposed in two parts, the model contribution and the coherent part, which comes from the transient solution. Fig. 8 shows the contribution of the different terms at $x = 11$. On average the resolved and modeled parts of the Reynolds stresses make equal contributions, except behind the cylinder ($y = 0$–0.2) where the contribution of the coherent structures is highest, and this is consistent with the instantaneous plot, Fig. 14 that will be discussed later. In the stagnation region the coherent part vanishes, but the modeled part, R_{11}, remains too high and there is a lack of redistribution to the wall parallel component $\overline{v'^2}$. Thus, these defects are due to the model and not to the unsteady behavior. Note that no wall echo terms are used, as only the standard formulation is currently available and it is known to be inadequate for impinging flows.

3.2. Coarse 3D simulations

LES and T-RANS simulations have been performed on the same coarse mesh. Fig. 9 shows fine LES versus coarse LES. The latter gives results in good agreement with the fine calculation, which is quite surprising in view of the coarseness of the mesh shown in Fig. 3. This means that the turbulent structures, which contain most of the kinetic energy, are big enough to be captured with a coarse grid. This is promising for industrial calculation of various configurations of tube bundles. The RSTM is likewise not very sensitive to grid coarsening, but this was rather expected (Fig. 10). Finally there seems to be no advantage to the T-RANS approach versus LES, at least for this specific case. This observation should not be generalized since the LES show that the present flow

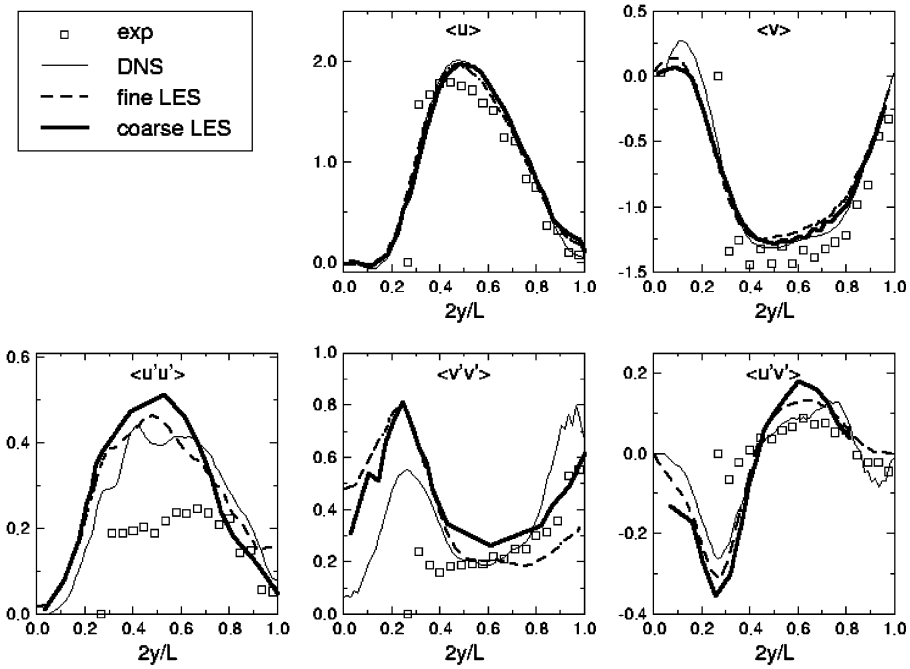

Fig. 9. Comparison of fine and coarse LES ($x = 11$).

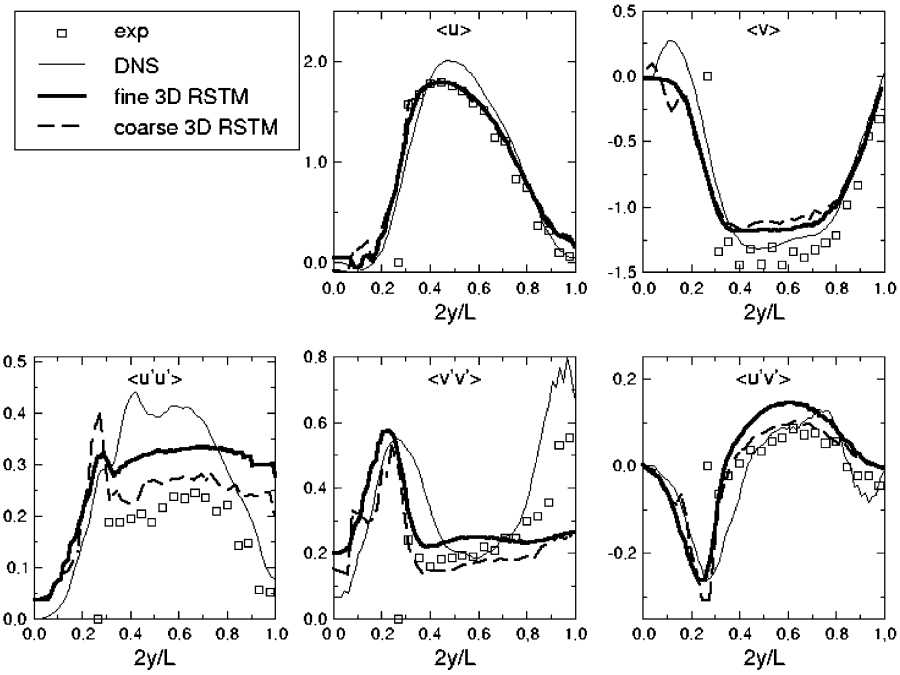

Fig. 10. Comparison of fine and coarse RSTM ($x = 11$).

is quite insensitive to near wall treatment, whereas in the T-RANS application of Kenjeres and Hanjalic (1999) the RSTM is essential in capturing the near wall complex phenomena.

3.3. 2D RSTM

The RSTM was in fact first tested in 2D with the fine mesh. An unsteady solution was obtained allowing us to compute statistics in the manner explained above. They are presented in Figs. 11 and 12 in which very severe overestimation of the normal stresses can be seen. It is almost entirely composed of the resolved contribution, and is due to the shedding of coherent 2D vortices from the cylinders. Even the mean velocity is affected, departing from the measurements. Note that this is in contrast with the successful 2D LES mentioned in the introduction, which however treated an "in line" tube bundle arrangement (Bouris et al., 2001).

3.4. Instantaneous fields

Fig. 13 shows an instantaneous velocity field with the 2D RSTM, for comparison with the 3D RSTM shown in Fig. 14. Animation shows a large quasi-periodic vortex shedding with the 2D simulation, however only very small ones are found in 3D. An animation of the 3D simulation shows that most of the large scale fluctuations are due to an oscillation of the flow around the cylinder, alternating between the left and right channels as was found in the LES of Rollet-Miet et al.

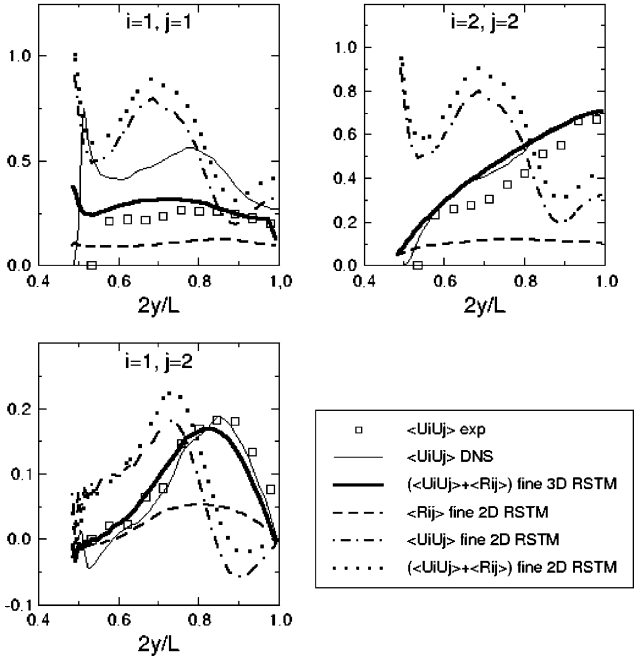

Fig. 11. 2D vs. 3D RSTM calculations—Reynolds stresses ($x = 0$).

Figs. 15 and 16 show isovalues of the total vorticity with the 3D RSTM and the LES. In the RSTM the resolved structures are clearly three-dimensional, which is inconsistent with the 2D assumption. In the upper part of Fig. 15 a large shedding vortex can be seen, but strong spanwise perturbations rapidly destroy it. It is certainly the lack of representation of this mechanism in

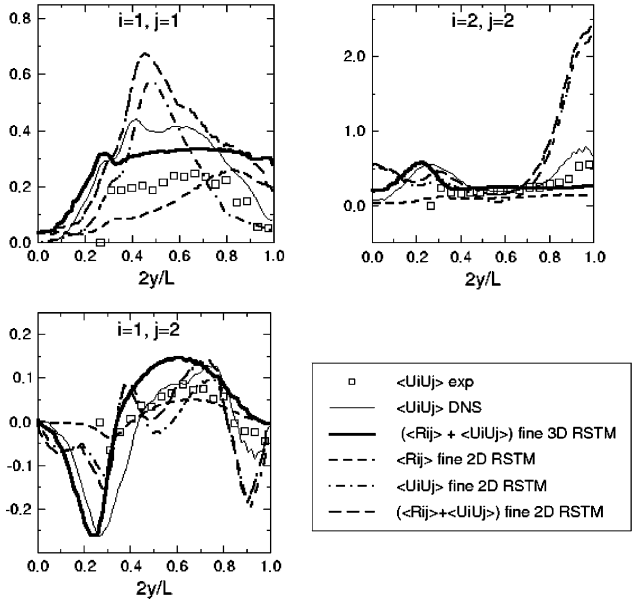

Fig. 12. 2D vs. 3D RSTM calculations—Reynolds stresses ($x = 11$).

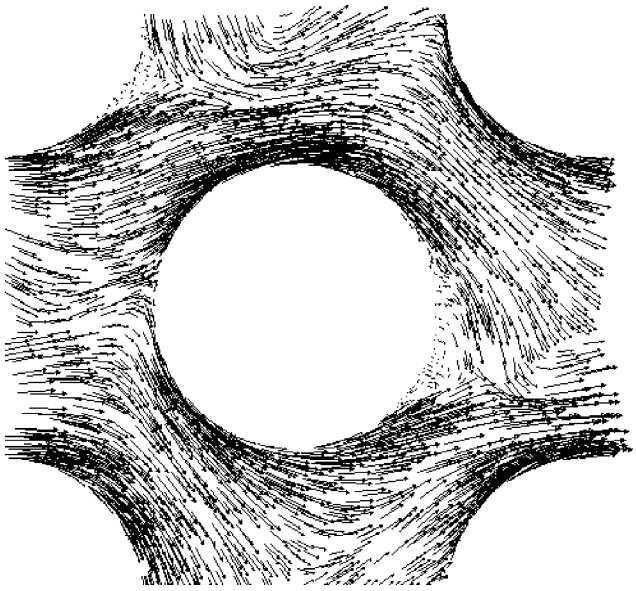

Fig. 14. Instantaneous velocity field—3D RSTM.

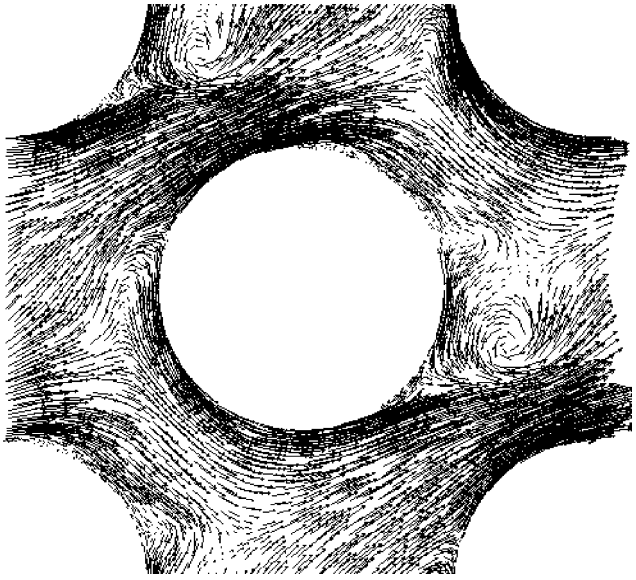

Fig. 13. Instantaneous velocity field—2D RSTM.

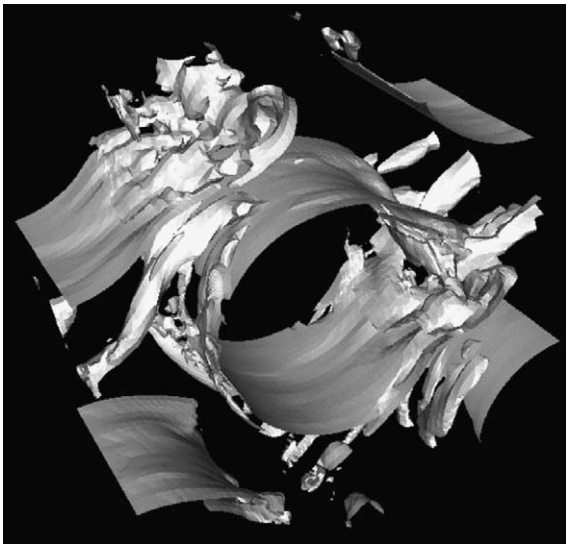

Fig. 15. Isovalues of the vorticity for the 3D RSTM (fine mesh) with an instantaneous velocity field.

the 2D simulation that is responsible for the poor results. For completeness Fig. 16 shows the instantaneous vorticity in the LES. A more sophisticated structure identification technique would be necessary to search for structures similar to those of Fig. 15.

The purpose of the present study of 2D RANS and coarse LES was to prepare parametric studies on a larger number of tubes for fluid-structure interaction analysis. A semi-empirical structure model currently used at EDF relies heavily on the assumed evolution of the lift coefficient as one of the tubes is parametrically displaced laterally. Clearly, an array of at least 4×4 tubes is then needed, as shown in Fig. 17. This mesh results in 1.3 Million nodes, which is significantly more demanding than the 2D URANS that was hoped to be used initially, but still amenable to parametric studies. It yields an intermediate mesh density, between that of the previous coarse and fine LES studied above. In following LES calculations the central tube will be given a series of out-of-line positions and the corresponding lift and drag values will be tabulated. In Fig. 18, the instantaneous flow-field shows no evidence a periodic pattern. This is somewhat reassuring, as the contrary would have required modeling an even larger array of tubes (since the periodic boundary conditions lead to

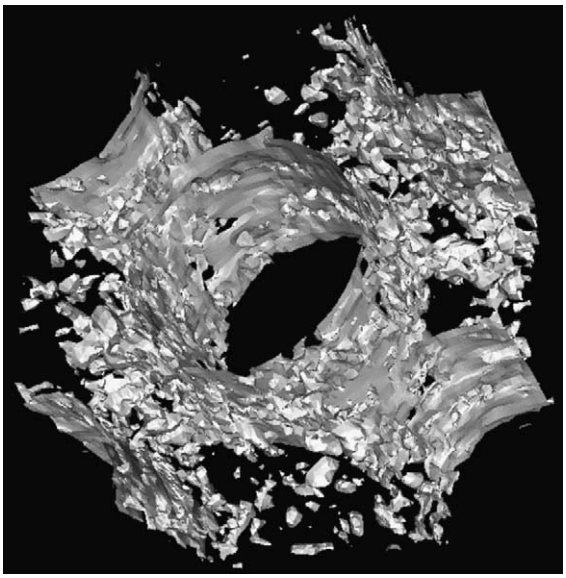

Fig. 16. Isovalues of the vorticity for LES (fine mesh) with an instantaneous velocity field.

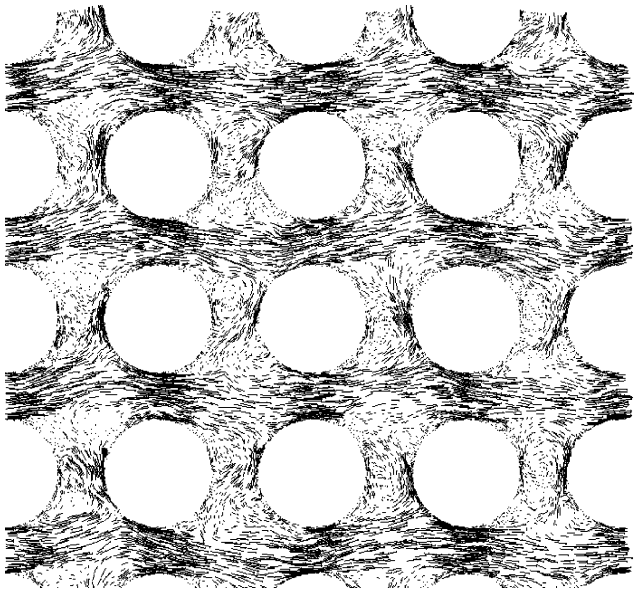

Fig. 18. Instantaneous flow-field showing no evidence a periodic pattern.

displacing one tube in every third row instead of the required single tube displacement).

4. Conclusion and perspectives

The LES and the RSTM (in a transient 3D approach) have been tested with two levels of grid refinement. Both approaches yielded satisfactory results with the LES being slightly more consistent with a DNS. A very coarse mesh produced good enough results for engineering purposes. This makes it possible to continue LES studies with more tubes to test the effect of the domain size, and also parametric simulations for different angles of attack and staggering (pitch/diameter). Another interesting point is the estimation of drag and

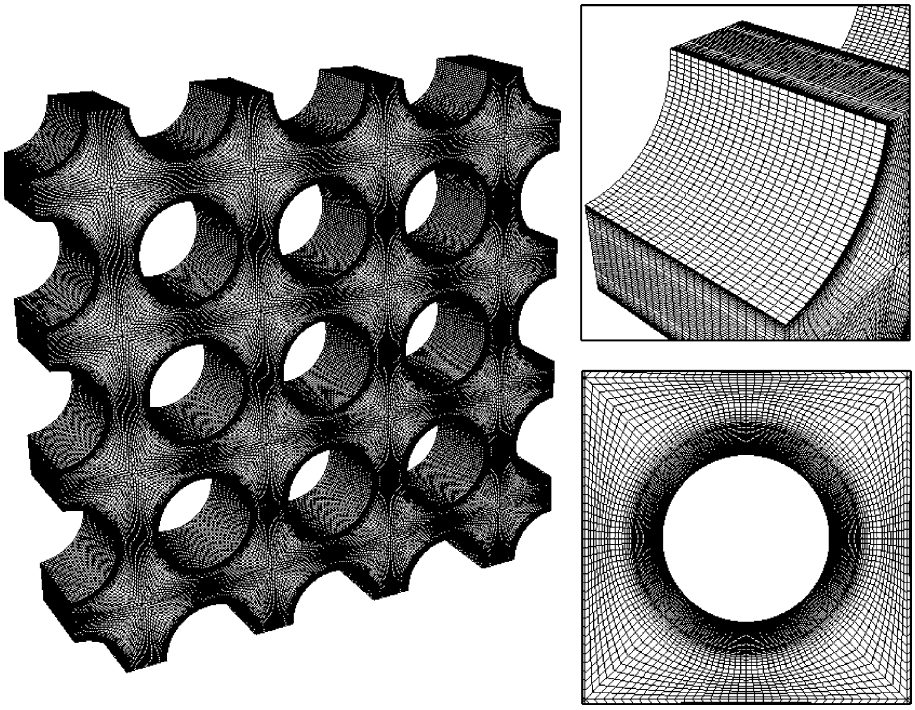

Fig. 17. Mesh of four by four tube array used for fluid-structure database.

lift coefficients when a tube is displaced, to create a database for fluid/structure interaction models.

The RSTM on a 2D mesh produced a severe overestimation of the total Reynolds stresses, which is explained by overly strong and persistent 2D vortices.

Further comparison of the unsteady RSTM with the LES in terms of structures and cut-off length scale is of theoretical interest, but the main conclusion is that no advantage of the RSTM over the LES was found, even when the mesh is made coarser and thereby laying more emphasis on the quality of modeling of the unresolved component of the turbulence.

Acknowledgements

The authors are very thankful to Pr. J.H. Ferziger for his advice on this paper, to Dr. T. Buchal for setting up the tube bundle test case, and to F. Archambeau and Dr. M. Sakiz for their contributions in developing *Code_Saturne*.

References

Archambeau, F., et al., 2003. A finite volume method for the computation of turbulent incompressible flows. Int. J Finite Vol., in preparation.

Bouris, D., Bergeles, G., 1999. Two dimensional time dependent simulation of the subcritical flow in a staggered tube bundle using a subgrid scale model. Int. J. Heat Fluid Flow 20 (2), 105–114.

Bouris, D., Papadakis, G., Bergeles, G., 2001. Numerical evaluation of alternate tube configurations for particle deposition rate in heat exchanger tube bundles. Int. J. Heat Fluid Flow 22 (5), 525–536.

Daly, B.J., Harlow, F.H., 1970. Transport equations in turbulence. Phys. Fluids 13 (11), 2634–2649.

Ferziger, J.H., Perić, M., 1999. Computational Methods for Fluid Dynamics, second ed. Springer, Berlin.

Gibson, M.M., Launder, B.E., 1978. Ground effects on pressure fluctuations in the atmospheric boundary layer. J. Fluid Mech. 86 (3), 491–511.

Hassan, Y., Ibrahim, W., 1997. Turbulence prediction in two-dimensional tube bundle flows using large eddy simulation. Nucl. Technol. 119, 11–28.

Kenjeres, S., Hanjalic, K., 1999. A T-RANS analysis of effects of body force and wall topology on coherent structures in turbulent flows. International Symposium on Turbulent Shear Flow Phenomena, Santa Barbara, USA.

Launder, B.E., Reece, G.J., Rodi, W., 1975. Progress in the development of a Reynolds stress turbulence closure. J. Fluid Mech. 68, 231–239.

Meyer, K.E., 1994. Experimental and numerical investigation of turbulent flow and heat transfer in staggered tube bundles, Ph.D. Thesis, AFM 94-03, Technical University of Denmark.

Moulinec, C., Pourquié, M.J.B.M., Boersma, B.J., Nieuwstadt, F.T.M., 2001. Diagonal Cartesian method on staggered grids for a DNS in a tube bundle, Direct and Large-Eddy, Simulation IV, Enschede, 2001.

Moulinec, C., Hunt, J.C.R., Nieuwstadt, F.T.M., in press. Disappearing wakes and dispersion in numerically simulated tube bundle flows. Flow Turbul. Combust.

Rhie, C.M., Chow, W.L., 1982. A numerical study of the turbulent flow past an isolated airfoil with training edge separation. AIAA paper, 82-0998.

Rollet-Miet, P., Laurence, D., Ferziger, J., 1999. LES and RANS of turbulent flow in tube bundles. Int. J. Heat Fluid Flow 20, 241–254.

Sebag, S., Maupu, V., Laurence, D., 1991. Non-orthogonal calculation procedures using second moment closures. Eighth Symposium on Turbulent Shear Flows.

Simonin, O., Barcouda, M., 1988. Measurements and prediction of turbulent flow entering a staggered tube bundle, Fourth International Symposium on Applications of Laser Anemometry to Fluid Mechanics, Lisbon, Portugal.

Werner, H., Wengle, H., 1991. LES of turbulent flow over and around a cube in a plane channel. Eighth Symposium on Turbulent Shear Flows.